

Seismic Behavior of Exterior RC Beam-Column Joints Retrofitted using CFRP Sheets

S. Y. Laseima^{a*} , A. A. Mutalib^{a*} , S. A. Osman^a , N. H. Hamid^b 

^a Faculty of Engineering and Built Environment, Universiti Kebangsaan Malaysia, Bangi Selangor, Malaysia.

E-mail: salehism555@siswa.ukm.edu.my; azrulaam@ukm.edu.my, saminah@ukm.edu.my

^b Institute Infrastructure Engineering and Sustainable Management, Universiti Teknologi MARA, Shah Alam, Selangor, Malaysia.

E-mail: norha454@uitm.edu.my

* Corresponding author

<http://dx.doi.org/10.1590/1679-78255910>

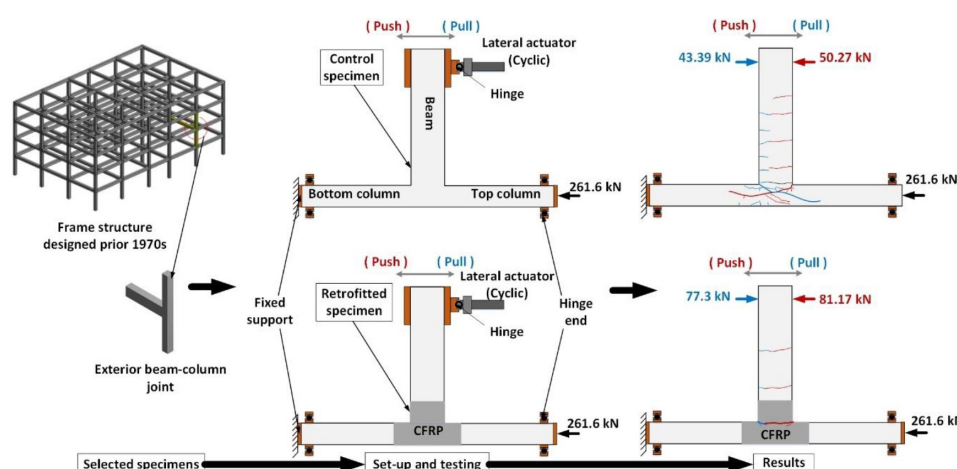
Abstract

The seismic behavior of full-scale exterior reinforced concrete (RC) beam-column joints retrofitted with externally bonded Carbon Fiber Polymers (CFRP) is examined in this paper. Casting and testing of two similar reinforced concrete beam column connections in the absence of transverse reinforcement at the joints took place under opposing cyclic loading with regulated displacement so as to examine their fundamental seismic performance. The first joint was examined as the control specimen and the other specimen was then retrofitted with CFRP sheets, with rounded border of the column and beam at and close to the joint region to change them from square to squircle segments. It is demonstrated in the experimental findings that the retrofitted beam column joint shows significantly greater strength, energy dissipation and ductility in comparison to the control specimen. There was a shift in the failure from the joint region to the beam ends in the retrofitted specimens, which would help in preventing the structure from disintegrating progressively. Because of the change in the beam and column from square to squircle segments, the debonding potential of the CFRP decreased and the restrictive impact of the CFRP increased. As a result, the experimental findings were verified using a 3D nonlinear finite element (FE) model. When the finite element and experimental findings are compared, it is determined that the suggested model is quite accurate.

Keywords

beam-column joint, CFRP sheets, squircle, cyclic loading, reinforced concrete

Graphical Abstract



Received: December 21, 2019. In Revised Form: March 13, 2020. Accepted: March 16, 2020. Available online: March 27, 2020

<https://doi.org/10.1590/1679-78255910>



Latin American Journal of Solids and Structures. ISSN 1679-7825. Copyright © 2020. This is an Open Access article distributed under the terms of the Creative Commons Attribution License, which permits unrestricted use, distribution, and reproduction in any medium, provided the original work is properly cited.

1 INTRODUCTION

Generally, the reinforced concrete frame buildings that were developed before the contemporary seismic codes were not in accordance with the requirements of the existing design codes (Sharma et al., (2010), Bai et al. (2003)). It was determined that a major reason of seismic vulnerability was joint shortcomings. The design of the buildings and structures was not for lateral loads, and so several of them fell down without any prior signs. Earthquakes across the globe in the previous few decades have shown that the reinforced concrete beam column joints are vulnerable to seismic loading ((Sezen et al. (2003), Dogangun (2004), Zhao et al. (2009), Alemdar and Sezen (2010)). The fragile detailed joints, particularly the external ones, have been recognized as crucial structural elements, and it seems that these collapse very soon. It is believed that weakness at joint is because of insufficient transverse reinforcement, and bond collapse of rebar takes place because of incorrect anchorage, faulty confinement and weak concrete ability (Paulay and Priestly , 1992)).

The most sustainable methods that can be used to enhance the security of reinforced concrete frame buildings are retrofitting and strengthening. There are several methods are that are used to improve the poor beam column joints, of which the most frequently used is the production of reinforced concrete or steel jackets. Steel cages were used by Alcocer and Jirsa (1993) to support RC frame connections, which included reinforced jackets and certain kinds of steel jackets. Extensive labor and accurate details are required in this approach. Furthermore, concrete jackets bring about an increase in the sizes and mass of structural components. Ghobarah et al. (1997), Paulay and Priestly (1992) also attempted to use plain or wavy steel plates. In addition, there are some areas that need special bonding to secure against corrosion, by using Epoxy adhesives with suitable bolts or special plaster.

One of the easiest and most cost-effective strengthening techniques is using fiber-reinforced polymers (FRP) composites in the form of externally bonded reinforcement. The benefits of FRP include high corrosion resistance, no impact on features of retrofitted/ restored member, large strength-to-weight ratio, little disturbance to building occupancy, simple applications and adaptability to various shapes (Gdoutos et al. (2000)). Furthermore, another advantage is the availability of design and application principles for practicing engineers (American Concrete Institution ACI, 2008). The efficiency of RC beam column joints is enhanced by FRP with respect to strength, energy dispersal and stiffness when seismic load is applied (Antonopoulos and Triantafillou, 2003).

Several experimental studies examined how FRP was successful in avoiding early shear failure of joints in the absence of internal confinement and altered the ability of joints to support yielding in the beam reinforcement (Gergely et al. (2000), Granata and Parvin (2001), Said and Nehdi (2004), Engindeniz et al. (2008), Pantelides et al. (2008), Le-Trung et al. (2010), Akguzel and Pampanin (2010), Alsayed et al. (2010)). It was shown in this study how FRP strengthening can effectively enhance the seismic behavior of poor RC beam-column joints. A total of 18 exterior RC beam column joints were examined by Antonopoulos and Triantafillou (2003) using a scale of 2:3. The part played by distribution and area fraction of FRP on shear strength of the joints was shown in this study. An experimental program was carried out by Ghobarah and Said (2001), El-Amoury and Ghobarah (2002), Mukherjee and Joshi (2005) to formulate useful selective rehabilitation structures for beam column joints. The part played by mechanical anchorages in restricting premature debonding with the help of sophisticated composite materials was shown in their study. A novel mechanism was formulated by Hadi and Tran (2014) to increase the seismic strength of below average reinforcing details of exterior beam-column connections by employing segmental circular concrete covers along with CFRP. It is demonstrated in the test findings that there was a significant increase in the shear efficiency of the retrofitted specimens and the column changed from square to circular sections, which decreased the debonding ability of the CFRP and increased the confinement impact of the CFRP. The use of various arrangements of the CFRP sheets to enhance the seismic efficiency of the joints by improving the sheer ability of non-seismic joints was evaluated by Le-Trung et al. (2010). It was demonstrated in the test results that when CFRP composites were correctly added to the non-seismic specimen, there was a significant increase in the lateral strength and ductility of the test specimens.

Al-Salloum and Almusallam (2007) and Almusallam and Al-Salloum (2007) performed experimental studies and assessments using simulated seismic loads to determine how effective the external bonds between CFRP sheets and concrete were in enhancing the sheer strength and ductility of beam-column joints. The behavior of retrofitted beam-concrete joints was studied by Beydokhty and Shariatmadar (2016). It was found that there were eight joints that were impaired, restored and strengthened with externally bonded CFRP sheets. The findings showed that this method brought about a considerable increase in energy dissipation and the overall performance, and hence, it is suitable for rehabilitating the seismic ability of the joints. It was examined by Hanoon et al. (2019) whether the CFRP-reinforcement method was effective in terms of energy absorption of two-span RC beams exposed to pure torsion. Torsional forces were imposed on 16 specimens; there were eight specimens that were not reinforced, while CFRP sheets were used to reinforce the rest of the eight specimens. The parameters that were examined were the impact of concrete compressive strength and the angle of a twist. It was demonstrated in the experimental findings that all beams covered with CFRP sheet presented

enhanced torsional energy absorption ability in comparison to the control specimens. This suggests that structural and material damages can be prevented by comprehending the energy absorption concept. A retrofit technology was created by (Del Vecchio et al., (2014), Truong et al., (2017)) by using cyclic loading that simulated earthquake loading to reinforce seven half-scale beam-column joint specimens. Several practical rehabilitation solutions were put forward in this study, which involved the use of carbon fiber reinforced polymer (CFRP) wrapping, steel jacketing, internally rooted head re-bars, and steel haunch components. The purpose of the study was to present an improved understanding of seismic performance of seismically extensive RC beam-column joints, which were reinforced with various retrofit materials. The shear strength of beam-column joints with light reinforcement details equipped with FRP systems were simulated using finite element method (FEM) (Del Vecchio et al., (2015), Pantazopoulou et al., (2016)). The way CFRP retrofitted with infilled RC frames function was examined by Sakr et al. (2017) using a finite element micro model. A four-node shell element was used in this study to model the concrete, infill panel and CFRP sheets. The interaction between concrete frame and infill panel was carried out using a contact surfaces model to permit the occurrence of separation and to avoid penetration. It was shown in the findings that the maximum efficiency of CFRP retrofitted infilled frame can be achieved by having bonding of around 25% of the diagonal length from either end so that similar behavior of the entirely bonded sheet can be achieved. A numerical study was carried out by Sabrin et al. (2018), in which non-linear static pushover method was used to analyze the seismic behavior of the actual moment that resisted RC frames. Distinct plastic hinge lengths and various concrete ultimate strain conditions of RC members were taken into account in the numerical modeling. The commercial software ETABS v. 9.6.0 was used to carry out the pushover assessment to examine the structural behavior of RC frames present in a seismic region. Pushover curves are used to find out seismic performance criteria with respect to ductility, over-strength and also response modification factor for frames. The analysis generally provides the load carrying ability and also the displacement at the highest lateral load and interstory drift index at any floor level of RC frames. The way the reinforced concrete (RC) beam-column joints function at the corner panel was examined by Abdelwahed (2019). In this study, the impact of deficiency in joints performance is numerically examined using distinct modeling methods, taking into account both seismic and non-seismic reinforcement details. It can be seen in the analysis that seismic detailing is appropriate for exterior and interior joints, which enhance the confidence that the numerical findings is attained by replicating identical behavior using distinct analytical techniques.

Several studies were carried out that concentrated on using FRP as a post-earthquake strengthening solution in extremely damaged joints, whereas there are limited studies that have examined the strengthening of structures that have not undergone any damage prior to earthquakes. It is important to achieve seismic reinforcement of weak structures prior to earthquakes to decrease risk and to ensure the safety of the lives and assets of those living in these structures. The focus of this study is on undamaged RC external joints of frame structures that were built before the contemporary seismic codes were established. Casting and evaluation of two similar specimens was carried out under cyclic loading to examine their fundamental seismic performance. Strengthening of the geometry and detailing of the testing specimens was carried out so that they would denote non-ductile detailed external joint of RC frame in accordance with the design of 1970s. One was taken to be the control specimen, while the other was later retrofitted with CFRP sheets. The former tests are the focus of this paper, and the seismic performance of the full-scale RC beam-column joints retrofitted with externally bonded CFRP is examined. Hence, the objective

of the tests was to examine the ability and performance of weak joints under cyclic loading, and determine successful strengthening ineffective joints by using FRP sheets. ANSYS 17 software was used to carry out the finite element modeling of the sub assemblage. Discussions of the experimental findings were carried out and were contrasted with the findings of the finite element model. Figure 1 illustrates the flow chart that shows the research methodology of the present study.

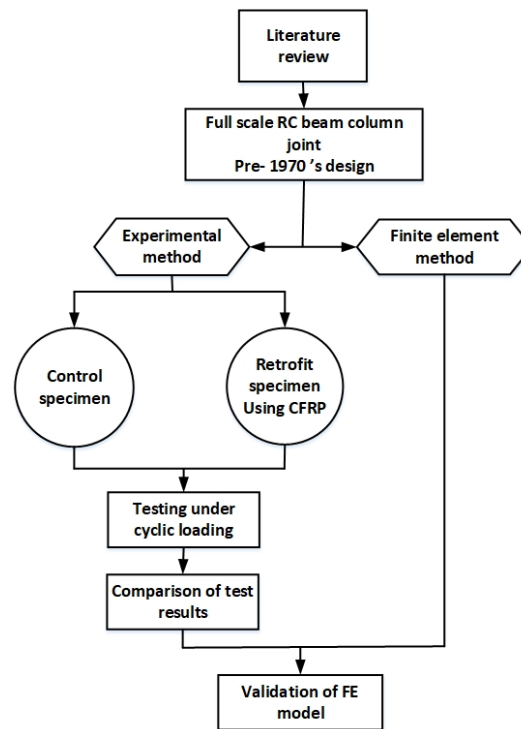


Figure 1: Research methodology flowchart.

2 MATERIALS AND METHODS

2.1 Description of the specimens

Casting and testing of two full-scale similar exterior reinforced concrete beam-column joints in the absence of joint transverse reinforcement detail at the joint region was carried out in this study, while applying cycling loading. Out of these, one was control specimen CS, while the other was externally reinforced using carbon fiber reinforced polymer (CFRP), having round edge of the column and beam at and close to the joint region to transform them from square to squircle segments. The study considered exterior beam column joint of a four-story strengthened concrete building of 12m in story height and three bays of 3.5m. The details of the building and the outer beam-column joint are depicted in Figure 2. There were similar connections, and these were prepared in the absence of any joint transverse reinforcement detail at the joints region to signify those connections that were constructed without taking into account the seismic impact. Figure 3 presents the dimensions and details of reinforcement applied to the specimens. The height of the column extended to 3000 mm, with cross-sectional dimensions of 250 * 250 mm. The length of the beam was 1625 mm from the surface of the column to the free end, with a cross-sectional area of 250 * 400 mm. The column was reinforced longitudinally with four $\phi 20$ mm bars with yield strength of 520 MPa, while the longitudinal reinforcement of the beam was carried out using three $\phi 16$ mm bars at the top as well as the bottom, having yield strength of 522 MPa. The stirrups of the column and the beam were carried out using $\phi 8$ mm plain bars, having yield strength of 305 MPa.

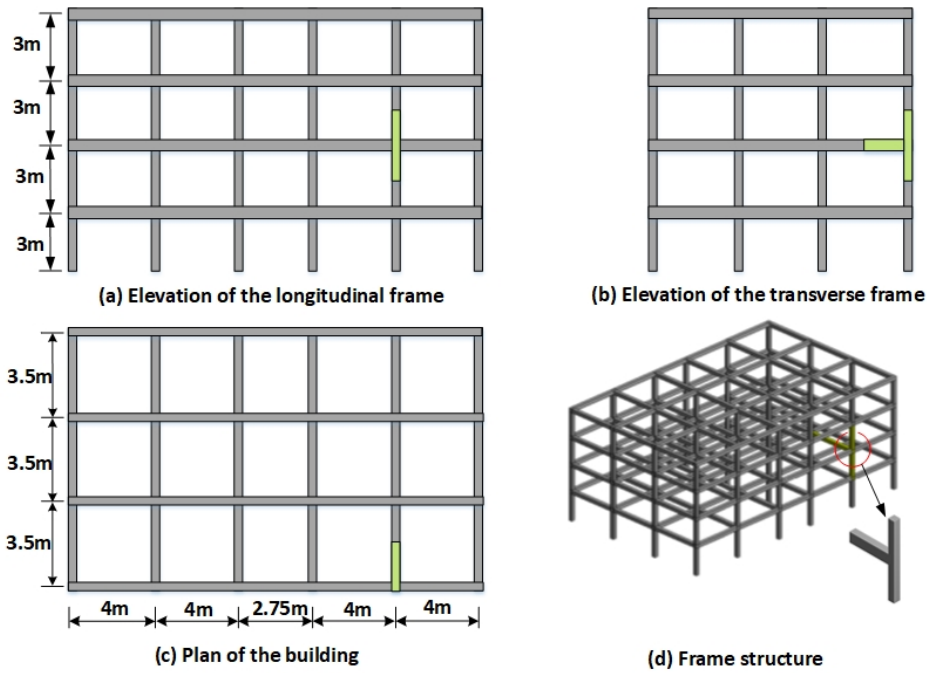


Figure 2: Specifications of the building.

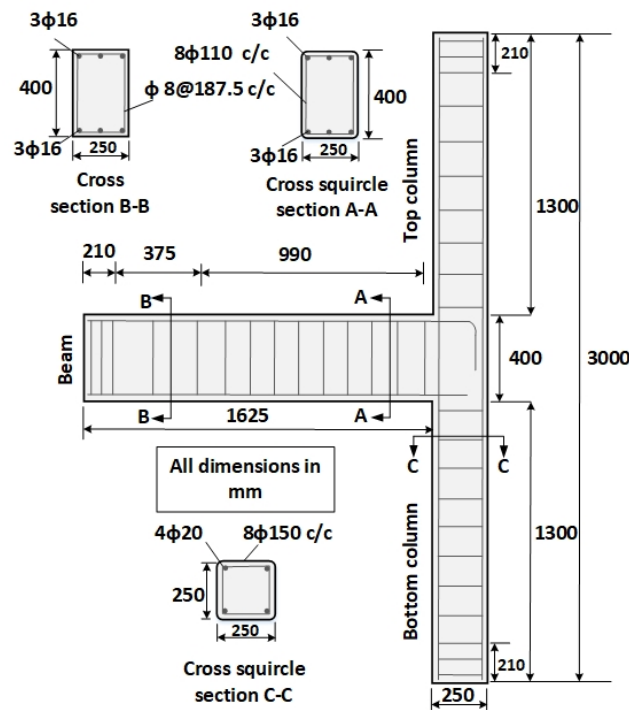


Figure 3: Specimen dimension and reinforcement specifications.

This study used Ordinary Portland cement Type I (OPC), local available sand filtered through a 2.36-mm sieve, coarse aggregate with the highest size of 10mm and water. Concrete for M30 grade was formulated. The British Department of Environment method (DOE Method of Concrete Mix Design) was followed when developing the mix design. This study considered a mix ratio of 1: 1.87: 2.19 with 0.5 water cement ratio to achieve the specified strength of M30. A water content of 213.33 kg/m³ and a cement content of almost 426.66 kg/m³ were used. The slump was recommended to remain between 30 to 60mm with this ratio of water to cement. Parts of plastic pipes were used at an extension of 250 mm from the column and beam surfaces at the top and bottom ends prior to casting for rounded edge of the column and beam, at and close to the joint area, and to change them from square to squircle sections. Figure 4 illustrates the plastic pipes parts prior to casting and the specimen following casting in the molds.



Figure 4: Plastic pipes parts before casting and the casted specimen in the moulds.

2.2 Design of CFRP sheets

The CFRP strengthening was designed considering the total shear capacity of the joint core as the sum of concrete and CFRP contributions. The concrete contribution (V_c) was computed according to ASCE/SEI 41-06 (2007), the shear capacity of the joint (V_c) is evaluated as follows in Eq. (1):

$$V_c = 0.083 \gamma b_j h_c \sqrt{f_c} \quad (1)$$

$$= 0.083(6)(250)(250)\sqrt{32.7} = 177.6 \text{ kN}$$

Where γ shear coefficient, f_c is the concrete compressive strength, and b_j and h_c are the effective joint width and the depth of the column in the direction of joint shear being considered, respectively.

The theoretical shear force required to develop the plastic capacity of the beam reinforcement V_{jh} was computed using force equilibrium according to Eq. (2). $P = 88.7 \text{ kN}$

$$V_{jh} = T_b - V_{col} = P \left[\frac{L_b}{jd} - \frac{L_b + 0.5 h_c}{H_c} \right] \quad (2)$$

$$= 88.7 \left[\frac{1445}{0.875(354)} - \frac{1445 + 0.5 (250)}{2700} \right] = 364.6 \text{ kN}$$

Where T_b is the tension force of the top beam reinforcement; V_{col} is the column shear; P is the applied load at beam, L_b is the beam length to the applied load point; d the effective depth of the beam, H_c is the distance between column supports and h_c is the height of the column cross section.

Thus, the shear to be resisted by the CFRP sheets V_f is:

$$V_f = V_{jh} - V_c \quad (3)$$

$$= 364.6 - 177.6 = 187.0 \text{ kN}$$

The required number of CFRP layers was determined using ACI 440.2R-08 guidelines (ACI Committee 440 2008) adopting the recommended value of effective CFRP strain ($\epsilon_{fe} = 0.004$). The required number of CFRP layers (n_{frp}) is evaluated as follows in Eq. (4):

$$n_{frp} = \frac{V_f}{\left[\frac{(2t_f \epsilon_{fe} E_f d_{fv})(\sin\alpha_1 + \cos\alpha_1) + (2t_f \epsilon_{fe} E_f d_{fv})(\sin\alpha_2 + \cos\alpha_2)}{(2t_f \epsilon_{fe} E_f d_{fv})(\sin\alpha_3 + \cos\alpha_3)} \right]} \tag{4}$$

$$n_{frp} = \frac{V_f}{\left[\frac{2t_f \epsilon_{fe} E_f d_{fv}((\sin\alpha_1 + \cos\alpha_1) + (\sin\alpha_2 + \cos\alpha_2))}{(\sin\alpha_3 + \cos\alpha_3)} \right]}$$

Where $\alpha_1 = 90^\circ$, $\alpha_2 = 32^\circ$ and $\alpha_3 = 148^\circ$ (as shown in figure 5)

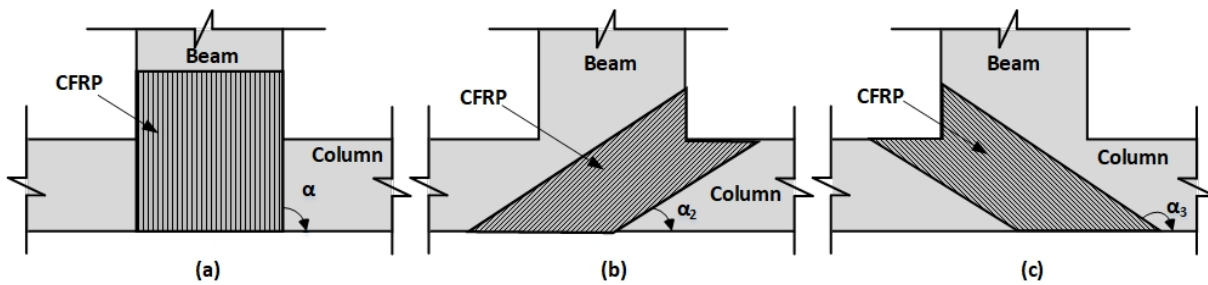


Figure 5: Illustration of angle α used in shear-strengthening calculations.

$$n_{frp} = \frac{187000}{\left[\frac{2(0.13)(0.004)(223000)(221)((\sin 90^\circ + \cos 90^\circ) + (\sin 32^\circ + \cos 32^\circ) + (\sin 148^\circ + \cos 148^\circ))}{(\sin 32^\circ + \cos 32^\circ) + (\sin 148^\circ + \cos 148^\circ)} \right]}$$

$$n_{frp} = 1.77 \text{ Layer} \approx 2 \text{ Layers}$$

Where t_f is thickness of CFRP, E_f is the modulus of elasticity of the CFRP and d_{fv} is the effective depth of CFRP shear reinforcement.

2.3 Shape and method for reinforcing exterior beam-column joint

There was U-shaped strengthening of the retrofitted cases surrounding the three sides of joint, with extension in the beam distance equivalent width of column, followed by the X-shaped reinforcement surrounding the joint. The sheets are inclined towards the horizontal axis of the beam at an angle close to the main direction of the stresses within the joint, with one strip being added at the end of the X-shaped strengthening sheets on the beam and two strips at the extremes of the X-shaped strengthening sheets on the column to avoid preliminary delamination. Figure 6 demonstrates the strengthening shape of the specimen surrounding the joint. The specimen of this study was reinforced using a 0.13 mm thick SikaWrap-231C unidirectional CFRP fabric sheet and a Sikadur-300 adhesive material (epoxy). CFRP sheet had the following properties: tensile strength of 2864.0 MPa, elastic modulus of 223.2 GPa and ultimate strain of 1.28%. The nominal properties of epoxy were: tensile strength of 30 MPa, tensile elastic modulus of 4.5 GPa and elongation at break of 0.9%, as shown in the manufacturer data sheet. The beam column joint was developed before the CFRP was fixed by using a grinding machine to grind all the side surfaces. This was done to ensure that there was greater contact between CFRP layer and concrete surface. After this, an air nozzle was used to clean the side surfaces of the joint and then wiped to remove any leftover dustover particles. In accordance with the instructions of the manufacturer, there will be automatic premixing of Resin Part A and hardener Part B of the two-component Sikadur-330 for 3 minutes, or till it becomes homogenous. The manufacturer asserted the ratio of resin and hardener mixture to be 4:1. A coat of Sikadur-330 primer was then applied on all sides of the concrete with the help of a trowel, brush or roller. Sikadur-330 primer is an epoxy with low viscosity and cured with 100% solids polyamine. The precisely measured and cut pieces of SikaWrap-231C were then accurately applied over the concrete. SikaWrap-231C was immediately set over the epoxy resin coating, after which the resin was crushed through the roving of the fabric

using a plastic laminating roller. This will ensure that all of the SikaWrap-230C reinforcements are fully infused within the resin hardener mix. Another coat of epoxy hardener mix will then be applied over the SikaWrap-231C as the final layer. Air bubbles that were present over the epoxy/concrete or epoxy/fiber interface are removed. These steps were also carried out on the second layer of CFRP. Strengthened beam column joint was cured for at least two weeks at room temperature before testing the beam column joint.

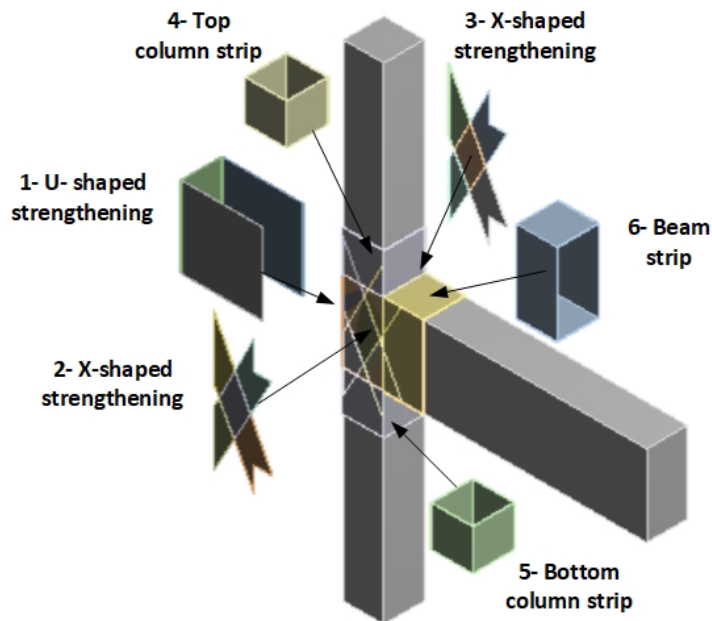


Figure 6: Strengthening of the specimen around the joint.

2.4 Test set-up and instrumentation

Testing was carried out on all the specimens in the column in horizontal position and the beam in vertical position, as depicted in Figure 7. The inflection points were simulated by pin-connecting at the left, right column ends and applying the beam tip in the loading plane. Cyclic load is applied over the beam tip, which is connected to an actuator with a swivel connector to use the lateral load. The same arrangement was employed in the two specimens to make sure that the results were consistent. Two hydraulic actuators were used to apply the load, which enable the axial and reversed quasi-static cyclic load to be applied. In the beginning, a 500 kN hydraulic jack was used to apply an axial load of almost 12.8% of the axial capacity of the column (261.6kN). It was believed that the axial load offered a feasible range in laboratory testing and also in actual frame constructions. A two-hinged actuator with a capacity of 500 kN was used to apply the lateral cyclic displacement (D) over the top of the beam in two opposing directions. A multi-cycle loading protocol that was based on Committee and American Concrete (2005) was used for the specimens of this study.

The loading protocol included a series of cycles, in displacement-control steps, where target drift reversals were represented as a function of drift ratio (DR%) in accordance with the loading history presented in Figure 7.

DR% refers to the percentage of lateral drift over the tip of the beam (over which the actuator load was applied) to the beam length, in addition to half of the column depth ($h_c/2$). Hence, loading steps with drift ratios (DR%) start at 0.01% in each test, after which steps of 0.1%, 0.133%, 0.2%, 0.4%, 0.5%, 0.75%, 1.0%, 1.25%, 1.5%, 1.75%, 2.0%, 2.5% occur till failure. There were two cycles in each loading step to examine the loss of strength and stiffness of the specimens that occurred in the recurring cycles. 100mm Linear Variable Differential Transducers (LVDTs) was used to determine the beam-tip displacement, column displacement, joint rotation and curvature along the beam.

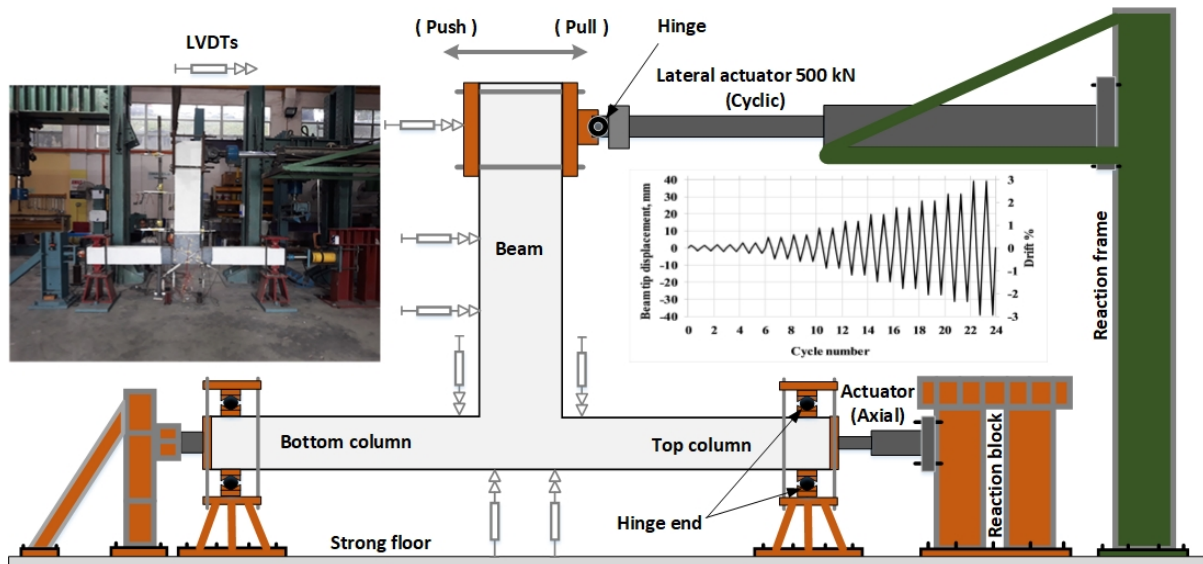


Figure 7: Test set-up and load history for the reversed cyclic load test.

3 RESULTS AND DISCUSSIONS

3.1 General

The results of the test units are discussed, along with the crack patterns. In addition, plots of the responses obtained are shown as applied displacement and load configurations. Furthermore, stiffness degradation, energy dissipation and Equivalent Viscous Damping Ratio properties are also created and reviewed to determine the performance.

3.2 Cracking pattern

3.2.1 Control specimen (CS)

Cracking was initially seen at the fourth load step, where there was load of +26.31 kN and displacement of +3.46 mm (DR% = +0.4%). The foremost shear link location of the beam was where the crack occurred. Similar cracks were seen on the two sides because of the load applied had a cyclic nature. When the load increased, further flexural cracks were seen across the beam at the shear link locations. When the load was +35.41 kN (DR% = +0.5%), the cracks first appeared in the core. These cracks started at the junction of the core and spread across the beam and column longitudinal reinforcement. A large diagonal shear crack occurred when the greatest capacity of the unit was attained at a load of +50.27 kN (DR% = +1.0%). Furthermore, flexural cracks were observed at the outer tension side of the lower column. After this, the application of loading shifted to displacement control and the assembly increased to a DR% of +0.75%. When cycling in opposing direction, various diagonal shear cracks surfaced in the core and an X-shaped failure mechanism developed, which caused the joint resistance to decrease. When the displacement increased more than the DR of -1.75%, the cracks extended and there was a significant decrease in the load. When the displacement became -35.92 mm (DR% = -2.0%), the test concluded. Figure 8 demonstrates the ultimate damage state and cracking pattern.

3.2.2 Retrofitted Specimen (CFRP)

It was at the fourth load step that the foremost cracking took place at a load of +19.32 kN and displacement of (DR% = +0.2%). The flexural cracks were observed from the middle part of the beam to close to the joint. Identical cracks were noticed on the two sides because of the cyclic nature of the applied load. When the load increased, a greater number of flexural cracks surfaced across the beam at shear link locations. At the lower end of the beam of joint, de-bonding of CFRP occurred at the seventh load step, with the load being +68.85 kN (DR% = +1.0 %). De-bonding also took place at the top part of the beam at the seventh reverse cycle, when the load applied amounted to -67.02 kN. A significant flexural crack was observed on the upper and lower corner of beam when the highest capacity of the unit attained a load of +81.22 kN (DR% = +1.5%). When the displacement increased to more than the DR of -2.0%, the size of the cracks increased, with a gradual decrease in the load. The test ended when displacement of -36.4mm was attained (DR% = -2.5%). Figure 9 demonstrates the ultimate damage state and cracking pattern.

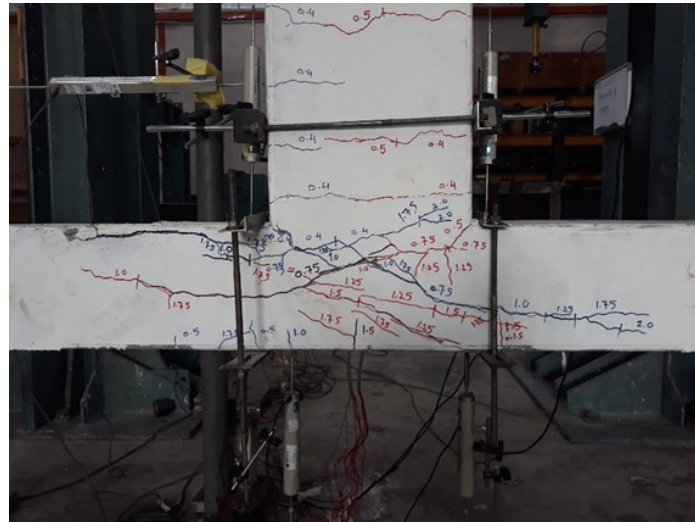


Figure 8: Final damage state and cracking pattern for CS specimen.

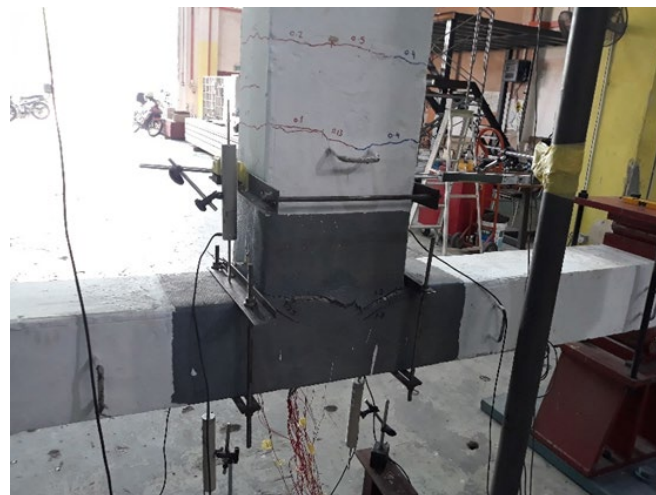


Figure 9: Final damage state and cracking pattern for CFRP specimen.

3.3 Hysteretic behaviour

Analysis and comparison of the hysteretic behavior of the joints in terms of load-displacement has been carried out in this section. The envelopes of load displacement hysteretic curves of the control specimen CS and retrofitted specimen CFRP has been presented in Figure 10, which shows the relationship between the peak loads at every cycle and the respective displacement. There was a significant increase in the lateral strength for retrofitted specimen CFRP, which was 61.7% more than the controlled specimen. The reason for the increase in the flexure strength is the confinement offered by CFRP. It also needs to be acknowledged the strain hardening is attained by the longitudinal reinforcement bars; as a result, the stress in the steel bars became more than the yield stress, causing the total strength of the retrofitted joints to increase.

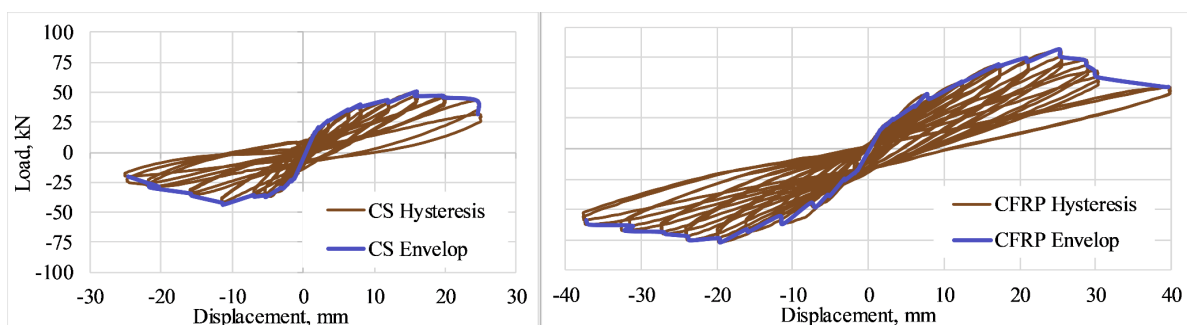


Figure 10: Hysteretic and envelop curves for CS and CFRP specimens.

3.4 Energy dissipation capacity

A key factor that can be used to assess the performance of column-beam joints on which seismic action has been carried out is the ability to disperse the inelastic deformation energy. The energy distributed by the specimen within an individual cycle, $E_i = \int P_i d\Delta$, was described as the area covered in the load-displacement hysteresis loop. It was then found that the total energy dissipated was the aggregate of the overall dissipated energy in each cycle of the test specimens. When the level of displacement increases, there is an increase in the energy dissipated in each cycle. The difference in the overall energy dissipation curves of the CS and CFRP specimens is demonstrated in Figure 11. In the ultimate stages of loading, it was noticed that there was a significant increase in CFRP specimen energy dissipation. CFRP retrofitted specimen absorbs 208.9% more energy in comparison the CS control specimen. In the initial three loading steps, very little energy was absorbed. Energy absorption continued to increase once the highest capacity was attained. When testing on the CFRP specimen concluded, an overall energy of 13025 kN.mm (DR= ± 2.5) was dissipated by the joint. At 0.5% DR, the joint dissipated 7% of the overall energy, at 1.0% DR, 22% of the energy was dissipated, at 1.5% DR, 49.8% of the energy was dissipated, at 2.0% DR, 82% energy dissipation occurred and finally, at 2.5% DR, there was 100% energy dissipation. These figures show that when there are minor variations of almost 1.0%, nearly the same overall energy was dissipated by both CS and CFRP specimens. After this, larger and more rapid energy dissipation was depicted by CFRP. The CFRP joint dissipated 50% of the energy at a DR of 1.25%, as compared to the CS. When the drifts were more than 1.25%, the per-cycle energy of the CFRP specimen became nearly 54% more than the value of the CS specimen all through the test.

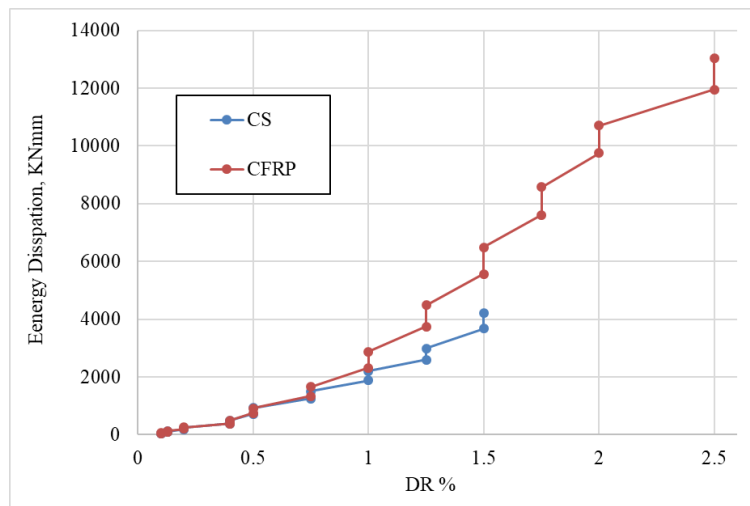


Figure 11: Cumulative energy dissipation curves of the specimens.

3.5 Ductility

A significant factor for earthquake resistant construction is ductility. To calculate the displacement ductility factor, the ratio of the final displacement related to a 10% strength degradation of the highest strength of the specimen (Li et al., 2002) to the displacement at the initial yield of internal steel or to the first crack is obtained. Table 1 shows the displacements at the initial yield of steel or at the foremost crack, final displacements, and displacement ductility factor for control specimen CS and retrofitted specimen CFRP. It can be seen that there is an increase in ductility of the retrofitted specimen CFRP by almost 61.8% in comparison to the control specimen CS.

Table 1: Displacement ductility factor for CS and CFRP specimens.

Specimen	Yield displacement Δ_y (mm)		Ultimate displacement Δ_u (mm)		Displacement ductility factor (μ)		Average displacement ductility factor (μ)
	Positive	Negative	Positive	Negative	Positive	Negative	
CS	3.46	2.86	15.85	11.31	4.58	3.95	4.27
CFRP	3.25	3.2	25.05	19.53	7.71	6.10	6.91

3.6 Stiffness degradation

The loss of stiffness across the loading cycles is used to determine the decrease in structural resistance to the seismic load. The increase in stiffness loss takes place at different rates, and the increase in peak displacement is represented by the decrease in the slopes of the load-displacement hysteresis loops. The peak-to-peak stiffness of the beam-tip load-displacement relationship is used to determine the stiffness, which is described as the slope of the line that joined the peak of the positive and negative response throughout the loading cycle (Saqa, 1995). Figure 12 shows that the preliminary stiffness of the control specimen CS is more than the retrofitted specimen CFRP, and with an increase in lateral sway, both the specimens lost their stiffness. In the beginning, the stiffness of the control specimen was almost 25% more than that of the retrofitted specimen. The figure shows that before a DR of $\pm 0.4\%$, the stiffness of the retrofitted specimen CFRP was the same as that of the control specimen CS. There was a decrease in stiffness because of the creation of diagonal cracks in the core ($DR=\pm 0.4$). After this, greater stiffness was exhibited by the retrofitted specimen all through the test. The same rate of stiffness degradation was exhibited by the two specimens following a DR of $\pm 0.4\%$. It was found that the retrofitted specimen CFRP exhibited less severe decrease in stiffness across the various loading steps. When the drift ratios were more than $\pm 1\%$, nearly twice the stiffness as the CS specimen was exhibited by the retrofitted specimen. The retrofitted specimen CFRP was found to depict somewhat greater stiffness in comparison to the control specimen CS and the largest stiffness in each loading cycle. The collapse behavior of the member is shown by the speed with which stiffness is lost.

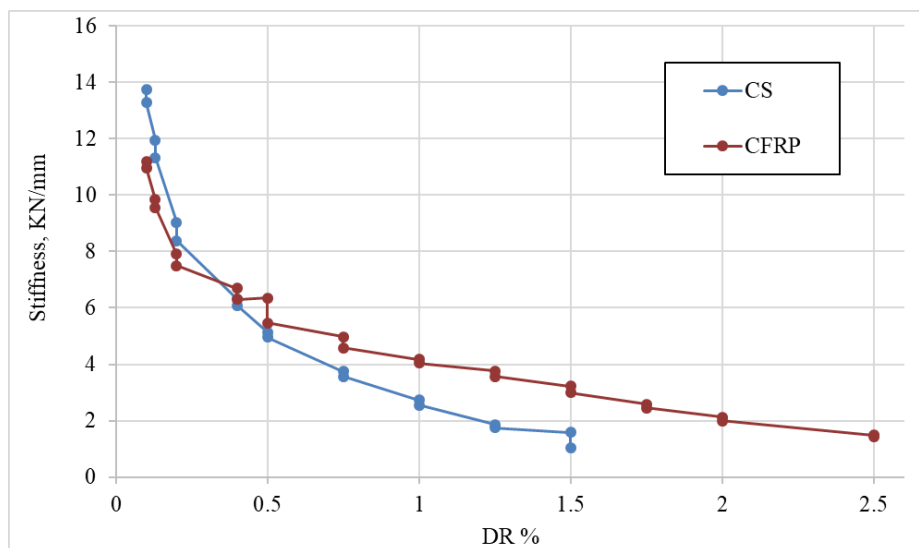


Figure 12: Stiffness Degradation of the specimens.

3.7 Equivalent viscous damping ratio

Besides reducing the structural damages by complementing either active or passive damper to the structures, the capacity of the structure to dissipate energy during an earthquake is referred to as the equivalent viscous damping (Symans and Constantinou, 1998). From the hysteresis loops acquired from tests, the area of one loop is used to calculate the amount of energy dissipated in one cycle of deformation. Moreover, the area under the triangle at maximum lateral load and displacement defines the elastic strain energy. According to (Chopra, 2011), the given below equation is used to calculate the equivalent damping:

$$\zeta_{eq} = \frac{E_D}{4\pi E_{SO}}$$

Where, E_D is the amount of energy dissipation per cycle; ζ_{eq} is the equivalent damping and the " E_{SO} " is the strain energy. Figure 13 presents the comparison between the Equivalent Viscous Damping ratio and the drift ratio of specimens CS and CFRP. It was observed that there were almost the same ratios for specimens CS and CFRP at 0.5% DR. This was because all specimens exhibited an elastic behavior till 0.5% DR. There were constant ratios for specimen CS at 0.75DR%, 1.0DR% and 1.25DR%, after which it began increasing. On the other hand, for the specimen CFRP, the ratios stayed the same from 0.75% till the final drift ratio of 2.5DR%.

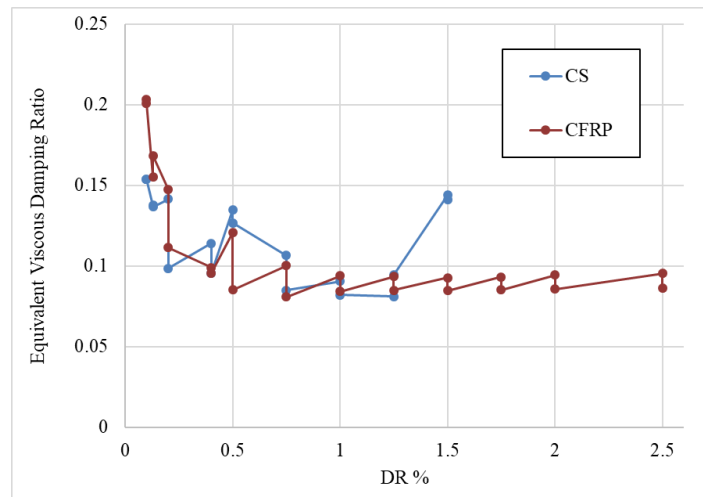


Figure 13: Equivalent Viscous Damping Ratio curves of the specimens.

3.8 Numerical Analysis (ANSYS)

The FEA (ANSYS) is carried out on the beam column joint that is made to undergo cyclic loading. 3-D modeling of solids is carried out using SOLID65 in the presence or absence of reinforcing bars (rebar), particularly developed for concrete that is able to deal with creep, plasticity, cracking in tension and squeezing in compression. There are eight nodes in the element, with three degrees of freedom at every node, having translations in the nodal x,y and z directions. The adopted element has non-linear properties that need an iterative solution. A series of two nodes link element (LINK 8) has been used to model the reinforcing steel. Eight-node multilayered solid element has been used to model the CFRP laminates (SOLID 46). Steel plates were included at support locations in the finite element models (just like in the actual specimens) to offer more equal stress distribution across the support regions and areas of applied load. It was presumed that the steel plates were linear elastic materials.

3.8.1 Boundary Conditions and Loading

The boundary conditions were simulated in the same way as in the test. Horizontal and vertical limitations, that signified a pin connection, were applied over the upper and lower ends of the column. Just the horizontal displacement was offered at the end beams to simulate the cyclic load conditions employed in the test. A consistent axial load of 261.6 kN was added to the upper end of the column. There was gradual application of the horizontal displacement at the beam end in a monotonic way.

3.8.2 Geometry and Finite Mesh

The choice of the beam and column mesh was such that the node points of the solid elements will correspond with the precise reinforcement locations. Laminate were modeled using solid elements, Solid 45, in the finite element model. Connections were established between the nodes of the solid elements (solid 45) and the neighboring concrete solid elements (solid 65) so as to achieve the ideal bond assumption. The steel reinforcement was signified by using Link 8 elements that are called link elements here. The bond strength between the concrete and the steel reinforcement should ideally be taken into account. This study, however, assumed that there was perfect bond between materials because of the constraints in ANSYS. A perfect bond can be offered when the link element for the steel reinforcement was linked between nodes of every surrounding concrete solid element so that the same nodes were shared between the two materials. Figure 14 depicts the finite element meshing of concrete, CFRP retrofitting and reinforcement in ANSYS. Figure 15 demonstrate the finite element outputs of control specimen CS at 0.1 DR% for concrete deformation, equivalent stress, reinforcement deformation and equivalent elastic strain.

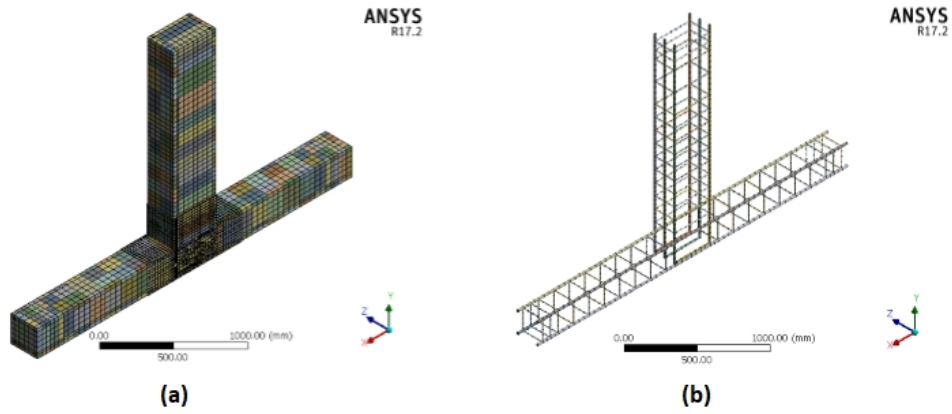


Figure 14: Finite element mesh of a) concrete and CFRP retrofitting, and b) reinforcement.

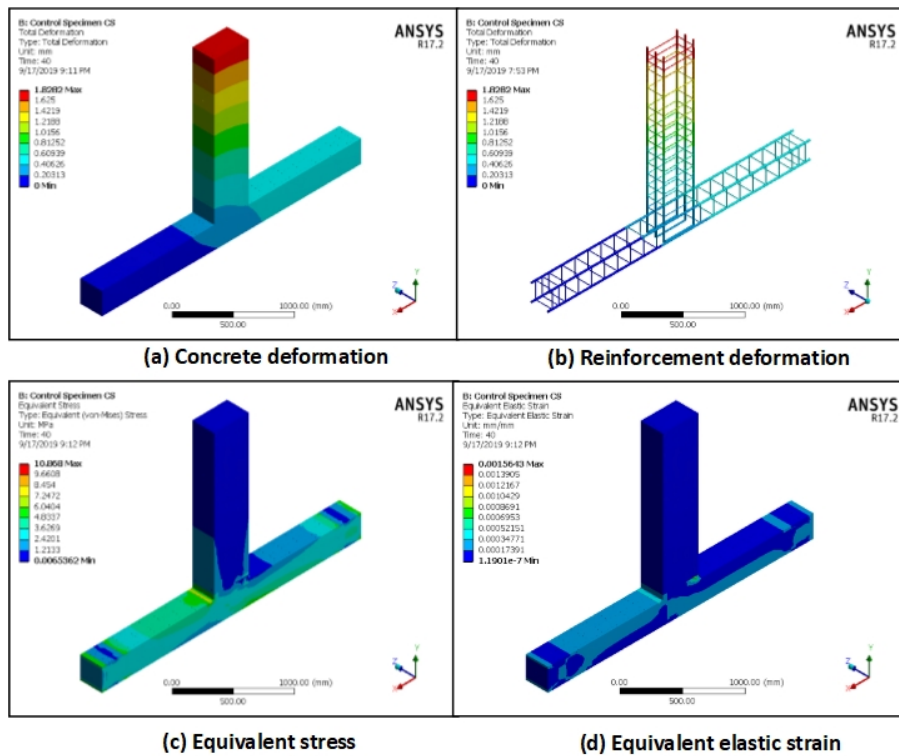


Figure 15: The finite element outputs of CS.

3.8.3 Control Specimen (CS)

Figure 16 presents a comparison of the hysteretic load-displacement relationship curves of analytical and experimental studies. An analysis of the hysteretic curves shows that when the displacement is 3.89 mm, the yield stress in the analytical solution is attained, with the highest displacement and load being around 17.8 mm and 54.0 kN, respectively. The experimental findings show that there is 3.46 mm displacement at yield and largest displacement of 15.85 mm, with the greatest load of 50.27 kN. It can be seen in the graph that there are similarities between numerical and experimental specimens. A difference of almost 10% is observed, which is attributed to the size of meshing and inherent complexity of non-linear modeling of hysteresis behavior.

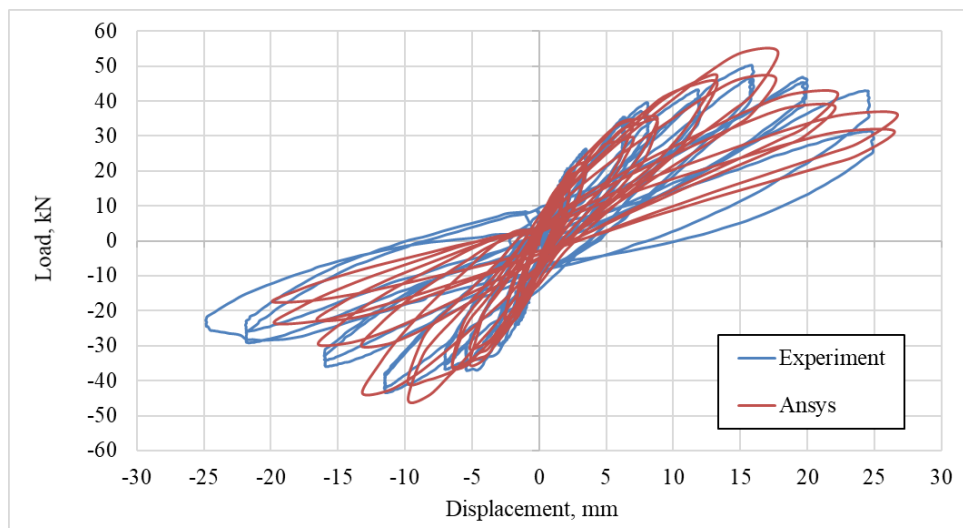


Figure 16: Experimental and analytical hysteretic load-displacement curve for CS.

Table 2 presents the cyclic behavior, stiffness degradation, energy dissipation and similar viscous damping ratio per cycle for analytical as well as experimental specimens.

Table 2: Energy dissipation, stiffness degradation and equivalent viscous damping ratio per cycle.

Drift %	Energy dissipation, kN.mm		Stiffness, kN/mm		Equivalent viscous damping ratio	
	Experiment	Ansys	Experiment	Ansys	Experiment	Ansys
0.10	28.54	19.22	13.73	11.00	0.15	0.12
0.10	53.02	36.47	13.27	9.56	0.15	0.13
0.13	88.57	67.11	11.95	10.08	0.14	0.15
0.13	118.51	101.97	11.33	9.79	0.14	0.18
0.20	194.02	168.12	9.04	7.79	0.14	0.15
0.20	247.19	226.59	8.38	7.22	0.10	0.15
0.40	383.75	361.65	6.32	5.82	0.11	0.10
0.40	499.43	483.02	6.09	5.07	0.10	0.11
0.50	725.46	691.71	5.13	4.77	0.13	0.12
0.50	929.73	922.09	4.96	4.67	0.13	0.14
0.75	1252.70	1224.07	3.75	4.12	0.11	0.09
0.75	1505.06	1621.63	3.57	3.78	0.08	0.13
1.00	1886.09	2063.59	2.73	3.17	0.09	0.09
1.00	2204.41	2409.61	2.56	2.45	0.08	0.09
1.25	2590.85	2816.73	1.87	1.85	0.08	0.09
1.25	2990.00	3161.59	1.75	1.55	0.09	0.09
1.50	3674.90	3568.53	1.58	1.27	0.14	0.09
1.50	4217.45	3899.26	1.05	1.03	0.14	0.09

Figures 17 and Figure 18 shows the differences in combined energy dissipation, stiffness and the Equivalent Viscous Damping ratio against drift ratio for analytical and experimental solutions. The overall collective energy dissipation is 3899.26 kN mm and 4217.45 kN mm in analytical and experimental studies, respectively. There was a decrease in the stiffness from 11.00 kN/mm to 1.03 kN/mm in analytical studies and from 13.73 kN/mm to 1.05 kN/mm in experimental studies. It can be seen in the graph that there are high similarities between numerical and experimental specimens. Till 1.25 DR%, the Equivalent Viscous Damping ratio against drift ratio for analytical and experimental solutions is almost the same. The analytical curve did not show any change after 1.0 DR%.

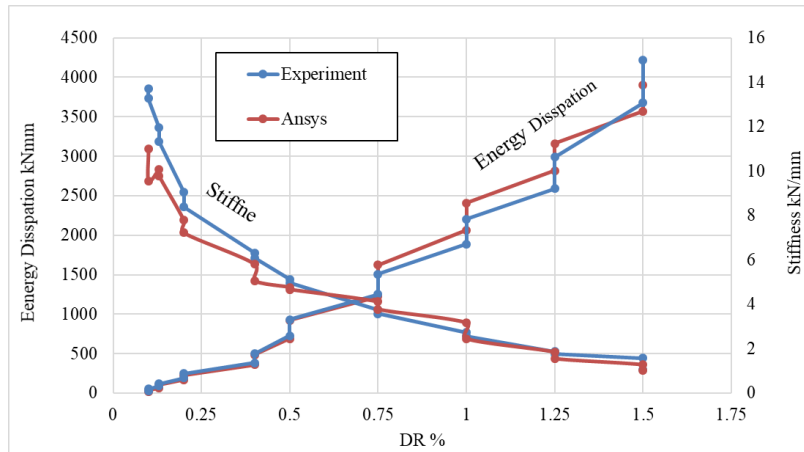


Figure 17: Collective energy dissipation versus stiffness for CS.

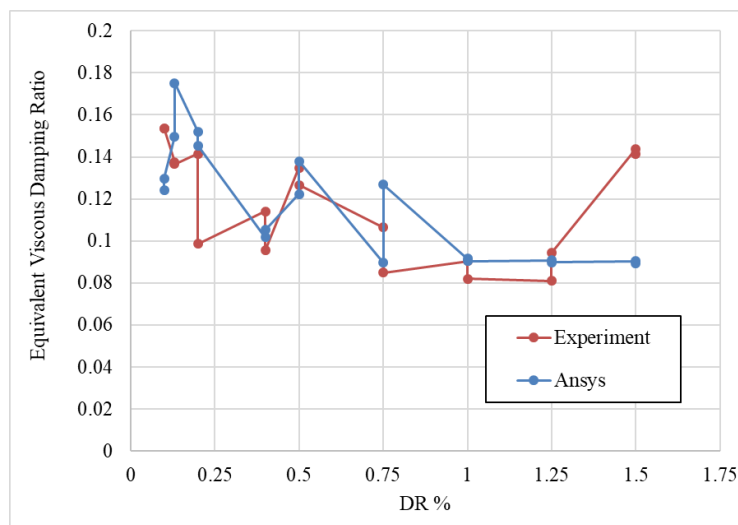


Figure 18: Equivalent Viscous Damping ratio versus drift ratio for CS.

3.8.4 Retrofitted specimen (CFRP)

Figure 19 shows the difference in hysteretic curves in analytical and experimental specimens. The first yield load of analytical and experiment curves is found to be relatively identical (3.25 kN), as well the highest load (81.2 kN). An identical trend for both experimental and numerical specimens is demonstrated by the curve, particularly in the positive region before the highest load. However, a few differences in the findings are observed following the highest load.

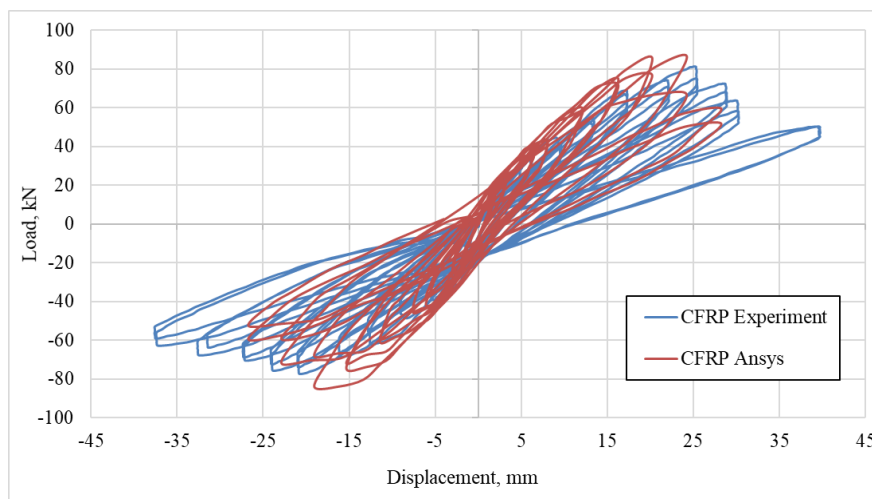


Figure 19: Analytical and experimental hysteretic load-displacement for CFRP.

Table 3 shows the cyclic behavior, decrease in stiffness, energy dissipation and identical damping ratio per cycle for analytical as well as experimental specimens.

Table 3: Energy dissipation, stiffness degradation and equivalent viscous damping ratio per cycle for CFRP.

Drift %	Energy dissipation, kN.mm		Stiffness, kN/mm		Equivalent viscous damping ratio	
	Experiment	Ansys	Experiment	Ansys	Experiment	Ansys
0.10	32.50	23.26	11.19	11.21	0.20	0.12
0.10	61.43	45.03	10.97	11.47	0.20	0.13
0.13	100.74	76.03	9.84	9.92	0.16	0.12
0.13	136.09	104.47	9.56	10.53	0.17	0.12
0.20	207.46	166.80	7.90	8.37	0.15	0.12
0.20	257.61	232.03	7.49	7.57	0.11	0.14
0.40	386.32	404.62	6.70	6.46	0.10	0.11
0.40	496.87	534.74	6.31	5.83	0.10	0.09
0.50	749.91	762.30	6.35	5.61	0.12	0.11
0.50	922.01	1039.47	5.46	5.51	0.09	0.13
0.75	1339.06	1526.04	4.98	5.11	0.10	0.11
0.75	1663.94	1951.42	4.58	4.98	0.08	0.10
1.00	2310.76	2650.66	4.18	4.74	0.09	0.09
1.00	2875.77	3380.94	4.04	4.55	0.08	0.10
1.25	3743.76	4394.39	3.77	4.32	0.09	0.10
1.25	4490.97	5160.58	3.56	3.69	0.09	0.09
1.50	5569.74	6382.47	3.22	3.36	0.09	0.10
1.50	6486.93	7450.64	3.00	2.68	0.08	0.11
1.75	7608.09	8433.07	2.59	2.17	0.09	0.10
1.75	8579.34	9383.97	2.45	1.90	0.09	0.11
2.00	9747.83	-	2.12	-	0.09	-
2.00	10706.26	-	1.99	-	0.09	-
2.50	11947.12	-	1.49	-	0.10	-
2.50	13025.81	-	1.43	-	0.09	-

Figures 20 and 21 demonstrate the combined energy dissipation, stiffness and the Equivalent Viscous Damping ratio against drift ratio of analytical and experimental studies. The analytical and experimental studies provide the values of overall collective energy dissipation as 9383.97 kN mm and 13025.81 kN mm, respectively. There was a decrease in stiffness from 11.21 kN/mm to 1.9kN/mm in analytical studies and from 11.19 kN/mm to 1.43kN/mm in experimental studies. It was found that analytical and experimental solutions had almost the same Equivalent Viscous Damping ratio against drift ratio. In each of the curves, a minor difference percent was recorded, which was because of the size of meshing and inherent complexity of non-linear modeling of hysteresis behavior.

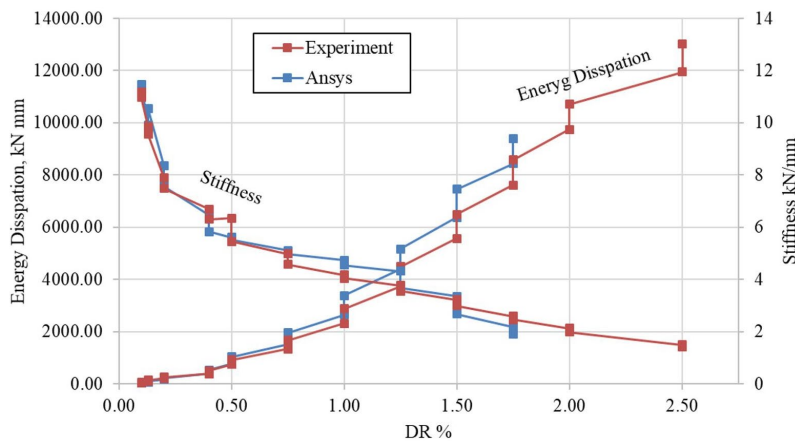


Figure 20: Experimental and analytical energy dissipation and stiffness of CFRP.

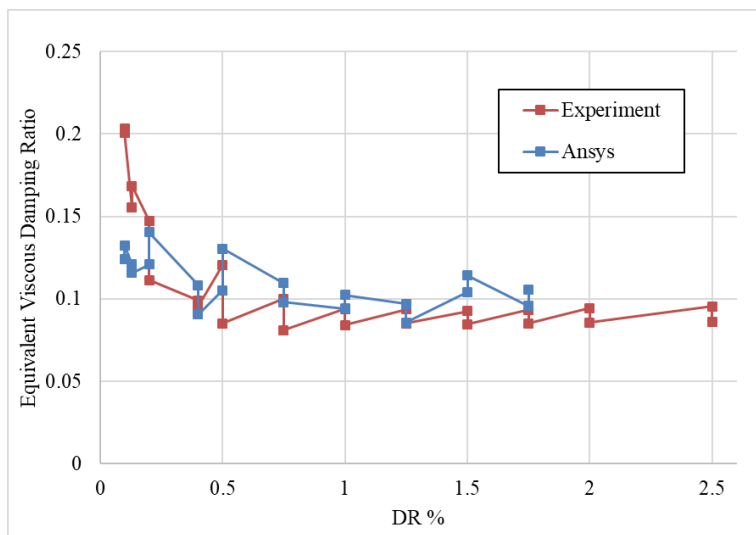


Figure 21: Equivalent Viscous Damping ratio versus drift ratio for CFRP.

The behavior of beam-column joints available in the literature was determined in the model. The data comprised of tests on external beam column joints carried out by Le-Trung et al. (2010). Eight external RC beam-column joint specimens were tested, comprising of a non-seismic specimen, a seismic specimen and six retrofitted specimens with distinct structures of CFRP sheets. The cross-sections of beam and column are 134mm X 200mm and 167mm X 167mm, respectively. The beam length from the column face is 1142mm and the column height is 968mm. The comparative findings of the study carried out by Le-Trung et al. (2010) and the numerical analysis findings achieved from the Finite Element Model (FEM) carried out in this study are shown in Table 4. The finite element analysis and experiment findings obtained are consistent with less than 15% variation, which may have been lower if a finer mesh had been used for simulation. However, it is presumed that the FEM model used is suitable for the objectives of the current study.

Table 4: The comparative results of the experiment and the numerical analysis results.

Specimen	Shape of strengthening	Ultimate load kN		Percentage difference %	Displacement at ultimate load, mm		Percentage difference %
		Experiment	Ansys		Experiment	Ansys	
NS	None	8.56	9.34	9.10	29.30	31.70	8.20
SD	None	10.42	11.49	10.30	23.00	25.16	9.40
RNS-1	T and L	10.10	11.44	13.30	29.15	32.21	10.50
RNS-2	T, L and strip on column	9.87	11.00	11.40	36.10	39.89	10.50
RNS-3	X	10.06	11.33	12.60	48.00	55.34	15.30
RNS-4	L and X	9.90	11.16	12.70	29.52	33.15	12.30
RNS-5	T, L and strip on column and beam	9.50	10.55	11.00	29.18	32.59	11.70
RNS-5	2T, L and strip on column	11.27	12.83	13.80	59.30	68.61	15.70

4. CONCLUSION

The key objective of this study is to formulate a successful retrofitting method for reinforced concrete beam column joint by using CFRP sheets to ensure that no damage and failure occurs in the joint area. Casting and testing of two similar specimens was carried out under cyclic loading to examine their fundamental seismic performance. Reinforcement was carried out on the specimens so that they denote non-ductile extensive exterior joint of RC structure in accordance with the design of the 1970s. Out of the two specimens, one was the control specimen, while the other was reinforced with CFRP sheets, having rounded edge of the column and beam at and close to the joint region to change them from square to squircle segments. A non-linear finite element analysis of the specimens was performed using ANSYS and the findings were contrasted with experimental findings with respect to cyclic behavior. The following deductions are made on the basis of detailed experimental analysis of beam-column joint:

- There is a significant improvement in the strength, energy dissipation and ductility capacity by 61.7%, 208.9% and 61.8% respectively due to retrofitting of beam-column joints using CFRP. This shows the suitability of using CFRP for retrofitting.
- It was shown in the findings of shear strength assessment in retrofitted specimen CFRP that the overall shear ability of this section is more than the demand recorded in the experiment. Hence, it was found that no shear damage occurred in the joint.
- When the edge of the column and beam was altered at and close to the joint region from square to squircle sections before CFRP reinforcement, the CFRP confinement impact was enhanced in this method and the debonding and bulging of CFRP at the joint center was removed, which made the application of CFRP more effective.
- Following the increase in the strength of the beam-column joint, there was a shift in the failure of retrofitted beam-column joint specimen from joint to the beam end. In addition, it was found there was no damage in the joint regions, which will ensure that the structures do not disintegrate gradually.
- It has been shown in the test findings that CFRP reinforcement causes the seismic performance of the weak RC beam column joints to improve.
- When the finite element is contrasted with the experimental findings, it is found that the suggested model is quite accurate.

Author's Contributions: Conceptualization, SY Laseima and AA Mutalib; Funding acquisition, AA Mutalib and SA Osman; Investigation, SY Laseima, AA Mutalib, SA Osman and NH Hamid; Methodology, SY Laseima and AA Mutalib; Resources, AA Mutalib and SA Osman; Software, SY Laseima and NH Hamid; Supervision, SY Laseima and AA Mutalib; Validation, SY Laseima and NH Hamid; Writing - original draft, SY Laseima, AA Mutalib, SA Osman and NH Hamid; Writing - review & editing, SY Laseima and AA Mutalib.

Editor: Marcílio Alves.

References

- Abdelwahed, B. (2019). Beam-Column Joints Reinforcement Detailing Adequacy in Case of a Corner Column Loss-Numerical Analysis. *Latin American Journal of Solids and Structures*, 16(7). doi:10.1590/1679-78255536.
- ACI Committee 440 (2008). ACI 440.2R-08 Guide for the Design and Construction of Externally Bonded FRP Systems for Strengthening Concrete Structures. American Concrete Institute, Farmington Hills, MI.
- Akguzel, U., & Pampanin, S. (2010). Effects of Variation of Axial Load and Bidirectional Loading on Seismic Performance of GFRP Retrofitted Reinforced Concrete Exterior Beam-Column Joints. *Journal of Composites for Construction*, 14(1), 94–104. doi:10.1061/(asce)1090-0268(2010)14:1(94).
- Al-Salloum, Y. A., & Almusallam, T. H. (2007). Seismic Response of Interior RC Beam-Column Joints Upgraded with FRP Sheets. I: Experimental Study. *Journal of Composites for Construction*, 11(6), 575–589. doi:10.1061/(asce)1090-0268(2007)11:6(575).
- Alcocer, S. M., & Jirsa, J. O. (1993). Strength of Reinforced Concrete Frame Connections Rehabilitated by Jacketing. *ACI Structural Journal*, 90(3). doi:10.14359/4185.
- Alemdar, F., & Sezen, H. (2010). Shear behavior of exterior reinforced concrete beam-column joints. *Structural Engineering and Mechanics*, 35(1), 123–126. doi:10.12989/sem.2010.35.1.123.
- Almusallam, T. H., & Al-Salloum, Y. A. (2007). Seismic Response of Interior RC Beam-Column Joints Upgraded with FRP Sheets. II: Analysis and Parametric Study. *Journal of Composites for Construction*, 11(6), 590–600. doi:10.1061/(asce)1090-0268(2007)11:6(590).
- Alsayed, S. H., Al-Salloum, Y. A., Almusallam, T. H., & Siddiqui, N. A. (2010). Seismic Response of FRP-Upgraded Exterior RC Beam-Column Joints. *Journal of Composites for Construction*, 14(2), 195–208. doi:10.1061/(asce)cc.1943-5614.0000067.
- Antonopoulos, C. P., & Triantafyllou, T. C. (2003). Experimental Investigation of FRP-Strengthened RC Beam-Column Joints. *Journal of Composites for Construction*, 7(1), 39–49. doi:10.1061/(asce)1090-0268(2003)7:1(39).

- ASCE/SEI 41-06 (2007). *Seismic Rehabilitation of Existing Buildings*. American Society of Civil Engineers, Reston, VA. doi:10.1061/9780784408841
- Bai, J. W., Center, M.-A. E., & Hueste, M. B. (2003). *Seismic retrofit for reinforced concrete building structures*. Mid-America Earthquake Center, CM-4.
- Beydokhty, E. Z., & Shariatmadar, H. (2016). Behavior of Damaged Exterior RC Beam-Column Joints Strengthened by CFRP Composites. *Latin American Journal of Solids and Structures*, 13(5), 880–896. doi:10.1590/1679-78252258.
- Chopra A.K. (2011). *Dynamics of Structures: Theory and Application to Earthquake Engineering*, Fourth Edition, ISBN No: 10:0132858037, Prentice-Hall.
- Committee, A. C. I. & American Concrete, I. (2005) Acceptance criteria for moment frames based on structural testing and commentary: an ACI standard, Farmington Hills, MI, American Concrete Institute.
- Del Vecchio, C., Di Ludovico, M., Prota, A., & Manfredi, G. (2015). Analytical model and design approach for FRP strengthening of non-conforming RC corner beam-column joints. *Engineering Structures*, 87, 8–20. doi:10.1016/j.engstruct.2015.01.013.
- Del Vecchio, C., Di Ludovico, M., Balsamo, A., Prota, A., Manfredi, G., & Dolce, M. (2014). Experimental Investigation of Exterior RC Beam-Column Joints Retrofitted with FRP Systems. *Journal of Composites for Construction*, 18(4), 04014002. doi:10.1061/(asce)cc.1943-5614.0000459.
- Dogangun, A. (2004). Performance of reinforced concrete buildings during the May 1, 2003 Bingöl earthquake in Turkey. *Engineering Structures*, 26(6), 841–856. doi:10.1016/j.engstruct.2004.02.005.
- El-Amoury, T., & Ghobarah, A. (2002). Seismic rehabilitation of beam-column joint using GFRP sheets. *Engineering Structures*, 24(11), 1397–1407. doi:10.1016/s0141-0296(02)00081-0.
- Engindeniz, M., Kahn, L.F., and Zureick, A.H. (2008). Performance of an RC corner beam-column joint severely damaged under bidirectional loading and rehabilitated with FRP composites. In: *Seismic Strengthening of Concrete Buildings Using Fiber Reinforced Polymer Composites*, T. Alkhrdahi and P. Silva, eds. ACI SP258-2.
- Gdoutos, A., Pilakoutas, K., and Rodopoulos, C. (2000). *Failure analysis of industrial composite materials*. McGraw-Hill Companies, NY, 51-108.
- Gergely, J., Pantelides, C. P., & Reaveley, L. D. (2000). Shear Strengthening of RCT-Joints Using CFRP Composites. *Journal of Composites for Construction*, 4(2), 56–64. doi:10.1061/(asce)1090-0268(2000)4:2(56)
- Ghobarah, A., Aly, N. M., & Attar, M. E. (1997). Performance level criteria and evaluation. *Seismic Design Methodologies for the Next Generation of Codes*, 207–215. doi:10.1201/9780203740019-19.
- Ghobarah, A., & Said, A. (2001). Seismic rehabilitation of beam-column joints using FRP laminates. *Journal of Earthquake Engineering*, 5(1), 113–129. doi:10.1080/13632460109350388.
- Granata, P. J., & Parvin, A. (2001). An experimental study on Kevlar strengthening of beam-column connections. *Composite Structures*, 53(2), 163–171. doi:10.1016/s0263-8223(00)00187-2
- Hadi, M. N. S., & Tran, T. M. (2014). Retrofitting nonseismically detailed exterior beam-column joints using concrete covers together with CFRP jacket. *Construction and Building Materials*, 63, 161–173. doi:10.1016/j.conbuildmat.2014.04.019.
- Hanoon, A. N., Abdulhameed, A. A., Abdulhameed, H. A., & Mohaisen, S. K. (2019). Energy Absorption Evaluation of CFRP-Strengthened Two-Spans Reinforced Concrete Beams under Pure Torsion. *Civil Engineering Journal*, 5(9), 2007–2018. doi:10.28991/cej-2019-03091389.
- Le-Trung, K., Lee, K., Lee, J., Lee, D. H., & Woo, S. (2010). Experimental study of RC beam-column joints strengthened using CFRP composites. *Composites Part B: Engineering*, 41(1), 76–85. doi:10.1016/j.compositesb.2009.06.005.
- Li, B., Wu, Y., & Pan, T.-C. (2002). Seismic behaviour of non-seismically detailed interior beam-wide column joints; part I: experimental results and observed behavior. *ACI Structural Journal*, 99(6). doi:10.14359/12344.
- Mukherjee, A., & Joshi, M. (2005). FRPC reinforced concrete beam-column joints under cyclic excitation. *Composite Structures*, 70(2), 185–199. doi:10.1016/j.compstruct.2004.08.022.
- Pantazopoulou, S. J., Tastani, S. P., Thermou, G. E., Triantafyllou, T., Monti, G., Bournas, D., & Guadagnini, M. (2016). Background to the European seismic design provisions for retrofitting RC elements using FRP materials. *Structural Concrete*, 17(2), 194–219. doi:10.1002/suco.201500102.

- Pantelides, C. P., Okahashi, Y., & Reaveley, L. D. (2008). Seismic Rehabilitation of Reinforced Concrete Frame Interior Beam-Column Joints with FRP Composites. *Journal of Composites for Construction*, 12(4), 435–445. doi:10.1061/(asce)1090-0268(2008)12:4(435).
- Paulay, T., & Priestly, M. J. N. (1992). *Seismic Design of Reinforced Concrete and Masonry Buildings*. John Wiley & Sons, Inc. New York. doi:10.1002/9780470172841.
- Sabrin, R., Siddique, M. A. A., & Sohel, M. K. (2018). Seismic Performance Assessment of Existing RC Frames with Different Ultimate Concrete Strains. *Civil Engineering Journal*, 4(6), 1273. doi:10.28991/cej-0309172.
- Said, A. M., & Nehdi, M. L. (2004). Use of FRP for RC Frames in Seismic Zones: Part I. Evaluation of FRP Beam-Column Joint Rehabilitation Techniques. *Applied Composite Materials*, 11(4), 205–226. doi:10.1023/b:acma.0000035462.41572.7a.
- Sakr, M., El-khoriby, S. R., Seleemah, A. A., & Darwish, E. A. (2017). FE Modeling of CFRP-Retrofitted RC Frames with Masonry Infill Walls. *Civil Engineering Journal*, 3(4), 267–287. doi:10.28991/cej-2017-00000090.
- Sagan, E. I. (1995). Evaluation of ductile beam-column connections for use in seismic-resistant precast frames. PhD thesis University of Texas, Austin.
- Sezen, H., Whittaker, A. S., Elwood, K. J., & Mosalam, K. M. (2003). Performance of reinforced concrete buildings during the August 17, 1999 Kocaeli, Turkey earthquake, and seismic design and construction practise in Turkey. *Engineering Structures*, 25(1), 103–114. doi:10.1016/s0141-0296(02)00121-9.
- Sharma, A., Genesio, G., Reddy, G., Eligehausen, R., Pampanin, S. & Vaze, K (2010). Experimental investigations on seismic retrofitting of reinforced concrete beam-column joints. 14th Symposium on Earthquake Engineering. Indian Institute of Technology, Roorkee. December 17-19, 2010. Paper No. A007
- Symans M.D. and Constantinou C.C. (1998). Passive fluid viscous damping systems for seismic energy dissipation. *ISET Journal for Earthquake Technology*, Paper No. 382, 35(4): 185-206.
- Truong, G. T., Dinh, N. H., Kim, J.-C., & Choi, K.-K. (2017). Seismic Performance of Exterior RC Beam-Column Joints Retrofitted using Various Retrofit Solutions. *International Journal of Concrete Structures and Materials*, 11(3), 415–433. doi:10.1007/s40069-017-0203-x.
- Zhao, B., Taucer, F., & Rossetto, T. (2009). Field investigation on the performance of building structures during the 12 May 2008 Wenchuan earthquake in China. *Engineering Structures*, 31(8), 1707–1723. doi:10.1016/j.engstruct.2009.02.039.